Analyst

Accepted Manuscript

ROYAL SOCIETY OF CHEMISTRY

www.rsc.org/analyst

Cite this: DOI: 10.1039/c0xx00000x

www.rsc.org/xxxxxx

COMMUNICATION

A naphthalimide based PET probe with Fe^{3+} selective detection ability: Theoretical and experimental study

Narendra Reddy Chereddy,*[a] M. V. Niladri Raju,[a] Peethani Nagaraju,[a] Venkat Raghavan Krishnaswamy,[b] Purna Sai Korrapati,[b] Prakriti Ranjan Bangal*[c] and Vaidya Jayathirtha Rao*[a]

Received (in XXX, XXX) Xth XXXXXXXXX 20XX, Accepted Xth XXXXXXXXX 20XX

DOI: 10.1039/b000000x

A naphthalimide based fluorescent probe '1' operates based on photoinduced electron transfer phenomenon is synthesized and its chemosensory application is explored. Among various metal ions, 1 selectively detects Fe^{3+} with a detection limit of 3.0 x 10^{-8} M. 1 is stable at physiological pH, non-toxic under experimental conditions and suitable for the detection of Fe^{3+} ions present in aqueous samples and live cells.

Iron, the most abundant transition metal in cellular systems, present in numerous number of enzymes and proteins and essential for various biological processes.[1] Iron acts as an oxygen carrier in haemoglobin and involved in several electron transfer reactions.[2] Owing to its redox nature (Fe^{3+}/Fe^{2+}), the labile iron in presence of reactive oxygen species can catalyze the formation of highly active oxygen derived free radicals *via* Fenton reaction.[3] The resultant highly reactive oxygen radical species can trigger protein oxidation, lipid peroxidation and DNA/RNA oxidation that can result in the development of pathology in diseases such as liver cirrhosis, cancer, neurodegeneration, hemochromatosis and hepatitis.[4] Hence development of new methods is necessary for tight monitoring of intracellular iron.

Recently great efforts have been made to develop new methods for Fe^{3+} detection. Techniques like atomic absorption spectroscopy,[5] colorimetry,[6] spectrophotometry,[7] and voltammetry[8] have been used for both qualitative and quantitative detection of Fe^{3+} ions. Digital fluorescence microscopy is advantageous over the above methods to monitor Fe^{3+} in biological systems.[9] Extensive research has been going on the development of fluorescent probes for the detection of intracellular iron. Since, Fe^{3+} is a fluorescence quencher due to its paramagnetic nature, most of the probes developed for Fe^{3+} detection are fluorescent 'turn-off' based.[10] Fluorescence 'turn-on' sensors are superior over 'turn-off' based in terms of sensitivity, hence research has been intensified in recent years to develop Fe^{3+} selective fluorescence 'turn-on' probes.[11]

Rhodamine and fluorescein fluorophores are widely explored to develop Fe^{3+} selective fluorescence 'turn-on' sensors, owing to their excellent photo-physical properties.[12] Apart from rhodamine and fluorescein, napthalimide is also an important fluorophore with good fluorescence quantum yield. Moreover, its fluorescence characteristics can be easily manipulated with simple chemical transformations.[13] Generally, incorporation of electron rich substituents like tertiary amines or pyridine rings

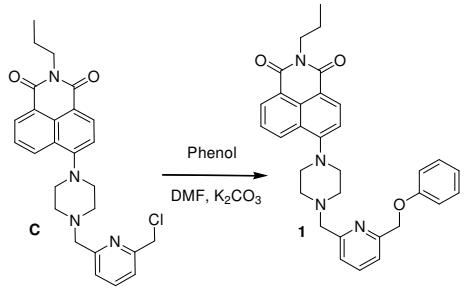

Scheme 1 Scheme for the synthesis of naphthalimide probe **1**.

(PET donors) onto the naphthalimide can quench its fluorescence *via* photoinduced electron transfer (PET) mechanism. The quenched naphthalimide fluorescence can be retrieved by reducing the electron donating capacity of PET donors, which is an advantageous factor for the development of fluorescent 'turn-on' metal ion chemosensors.[14] Utilizing this advantage, we have developed a naphthalimide based fluorescence 'turn-on' chemosensor with Fe^{3+} selective detection ability.

In the present manuscript, we report the design, synthesis and metal ion sensing properties of a naphthalimide based fluorescent probe **1**. The weakly fluorescent probe **1** switched to highly fluorescent, selectively in the presence of Fe^{3+} ions. The underlying reason for the observed Fe^{3+}-induced fluorescence changes in **1** is explored using DFT calculations and time resolved fluorescence studies employing time correlated single photon counting (TCSPC) technique. Cytotoxicity of the probe, effect of pH and other competitive metal ions on the Fe^{3+} detection ability of **1** are explored to evaluate the probe's applicability to image the live cells exposed to Fe^{3+} ions.

The naphthalimide based probe **1** was synthesized as shown in **scheme 1** and it is well characterised using NMR and ESI-HRMS analytical techniques (Figs. S1-S3, ESI†). The probe comprised a naphthalimide (signalling moiety) and a piperazine attached pyridine phenyl ether (metal coordination moiety) moieties. However the probe contained naphthalimide moiety, it exhibited weak fluorescence (Φ = 0.012) peaking at 518 nm in 1:1 v/v 0.01M Tris HCl-CH_3CN, pH 7.4 medium (**Fig. 1b**), which is in sharp contrast to the pure naphthalimide fluorescence. This excited singlet state quenching could be well rationalized by considering the intramolecular photoinduced electron transfer (PET) from piperazine 'N' to naphthalimide moiety.[14]

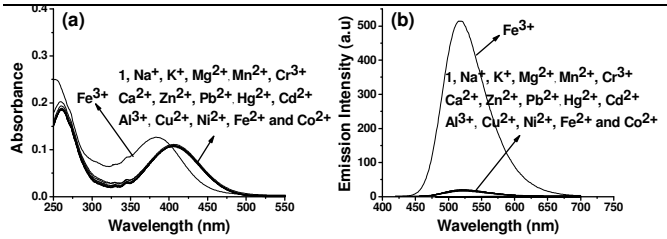

Fig. 1. Metal ion (20 μM) induced variations in the (**a**) absorbance, and (**b**) fluorescence spectra of **1** (10 μM); Excitation wavelength: 400 nm.

In order to identify the fusibility of PET process in **1**, its frontier molecular orbital energy levels were calculated using density functional theory (DFT) and time dependent density functional theory (TDDFT) calculations using Gaussian 03 package with B3LYP functional and 6-31G(D,P) basis set. The energetically optimized structure of **1** and its corresponding Cartesian coordinates are provided in Fig. S4, ESI†. The electronic transitions derived from TDDFT calculations on **1** and their corresponding oscillator strengths are provided in Table 1, ESI†. These results revealed that electronic transitions from HOMO to LUMO and HOMO-3 to LUMO have considerable contribution to state S1. Theoretically generated UV-visible absorption spectrum of **1** is shown in Fig. S5, ESI† and it is well matched with the experimentally obtained (**Fig. 1a**). The molecular orbital energy level calculations on **1** denoted that the energy of piperazine 'N' lone pair orbital (HOMO-2) was located above the HOMO-3 of the probe. This orbital arrangement permits electron transfer from piperazine 'N' (HOMO-2) to naphthalimide moiety (HOMO-3) and prohibits the electron comeback from LUMO of the naphthalimide and thereby quench its fluorescence (Fig. S6a, ESI†).[15] Hence, the results of DFT calculations indicated that the observed weakly fluorescent nature of **1** might be resulted from the PET from piperazine 'N' (HOMO-2) to naphthalimide moiety (HOMO-3).

However, the kinetic information pertaining the excited singlet state quenching of probe **1** was established using time resolved fluorescence studies. The fluorescence decay profile of **1** along with the instrument response function (IRF) is provided in **Fig. 2a**. As shown in **Fig. 2a** and Fig. S7, ESI†, the decay profile of **1** could be best fitted by bi-exponential function. The first component exhibited very fast decay time (τ_{fast} ~190 ps) with very high amplitude of ~99% and the second component showed very slow decay time (τ_{slow} ~ 7 ns) with 1% amplitude (Fig. S7, ESI†). The fast-decaying component could be assigned to the charge separation time, while the slower one is the natural lifetime of naphthalimide. Assuming the fast-decaying component was due to charge separation, the rate constant of charge separation state 'k_{cs}' was determined ($k_{cs} = 1/\tau_{fast} - 1/\tau_{slow}$) to be 5.12 x10 ^{9} s^{-1}. In agreement with the steady state fluorescence yield, the quantum yield for charge separation φ_{cs} [$\varphi_{cs} = (1/\tau_{fast} - 1/\tau_{slow}) / 1/\tau_{fast}$] was calculated to be > 97%. The observed very fast decay profile of **1** (nearly equal to IRF) clearly established the efficient PET process and it was also confirmed from the results of DFT calculations.

Metal ion chemosensory application of probe **1** was estimated in aqueous acetonitrile media (1:1 v/v 0.01M Tris HCl-CH_3CN, pH 7.4) using UV-visible and fluorescence analytical techniques. The weakly fluorescent probe **1** (10 μM) turned to highly fluorescent (Φ = 0.35) with enhanced emission intensity at ~518 nm, selectively upon addition of Fe^{3+} (20 μM) ions .The addition of other competitive metal ions (20 μM) like Na^{+}, K^{+}, Mg^{2+}, Ca^{2+}, Cu^{2+}, Cr^{3+}, Mn^{2+}, Co^{2+}, Ni^{2+}, Zn^{2+}, Cd^{2+}, Hg^{2+}, Fe^{2+} and Pb^{2+} has trivial impact on the fluorescence characteristics of **1** (**Fig. 1b**). Generally, addition of paramagnetic metal ions like Cu^{2+} and Fe^{3+} quenches fluorescence. However, the observed enhancement in the fluorescence intensity of **1** with the addition of Fe^{3+} might be ascribed due to the Fe^{3+}-induced reduction in the photoinduced electron transfer from piperazine 'N' to naphthalimide moiety. Under similar conditions, probe **1** (10 μM) alone displayed an absorption band centred at ~407 nm (ε = 11000 cm^{-1} M^{-1}) and it was impassive to the addition of various metal ions (20 μM) except Fe^{3+}, the addition of which shifted the absorption maxima of **1** to ~383 nm (ε = 12600 $cm^{-1}M^{-1}$, **Fig. 1a**). The observed Fe^{3+} selective blue shift in the absorption maxima of **1** indicated the involvement of piperazine 'N' attached to naphthalimide moiety in **1-Fe^{3+}** complex formation.

Job plot analysis was carried out to estimate the stoichiometry of **1-Fe^{3+}** complex and it was found to be 1:1 in nature (Fig. S8, ESI†). The 1:1 stoichiometry of **1-Fe^{3+}** complex was further confirmed using ESI MS data (Fig. S9, ESI†). The tri-positive **(1-Fe)$^{3+}$** complex was optimized using Gaussian 03 with B3LYP functional and 6-31G(D,P) basis set and the optimized structure and its corresponding coordinates are provided in Fig. S10, ESI†. Theoretically generated UV-visible absorption spectrum of **(1-Fe)$^{3+}$** complex is shown in Fig. S5, ESI†. The absorption band at 339 nm was resulted from the electronic transitions of the naphthalimide moiety and it is at shorter wavelength side compared to the experimentally observed (**Fig. 1a**). The results of the TDDFT calculations on **(1-Fe)$^{3+}$** complex revealed that the transition from HOMO-2 to LUMO has considerable contribution to state S1 (Table 1, ESI†). The combined results of the theoretical calculations on **1** and **(1-Fe)$^{3+}$** complex indicated that the molecular orbital energy levels of **1** were reduced upon complexed to Fe^{3+} and the reduction was much pronounced in the case of piperazine 'N' lone pair orbital. This sharp reduction in the energy of piperazine 'N' lone pair orbital prohibits the PET from piperazine 'N' to naphthalimide and hence enhances the fluorescence quantum yield of **1-Fe^{3+}** complex (Fig. S6b, ESI†).[15]

The Fe^{3+} induced reduction in PET in **1** was further confirmed using TCSPC experiments. **Fig. 2b** portraits the fluorescence decay profiles of **1** as a function of Fe^{3+} concentration. Upon successive addition of Fe^{3+} ions (0-100 μM) to **1** (100 μM), a gradual enhancement in the amplitude of slowly decaying component with a concomitant reduction in the amplitude of fast decaying component was observed by keeping the respective

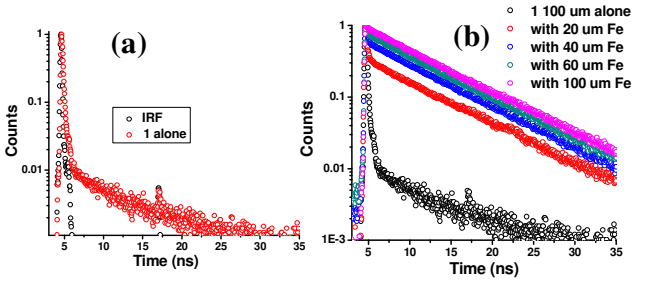

Fig. 2. Nano-second fluorescence lifetime decay profiles of **1** (**a**) and **1** with different amounts of Fe^{3+} (**b**).

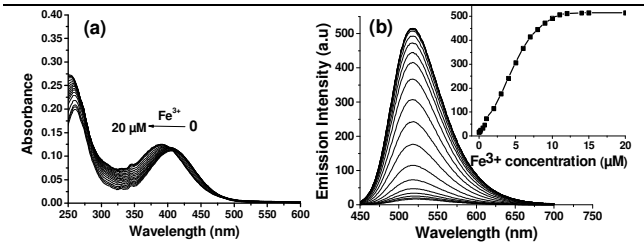

Fig. 3. The Fe^{3+} (0-20 μM) concentration dependent variations in the absorbance (**a**) and fluorescence (**b**) spectra of **1** (10 μM). Excitation wavelength was 400 nm.

decay times unaltered (Fig. S11, ESI†). The observed reduction and increment in the amplitudes of the fast and slow decaying components, respectively confirmed the conversion of charge separated state to florescent excited singlet state by the formation of **1-Fe^{3+}** complex. Lenoir response curves using the fluorescence lifetime data were plotted to determine the lower detection limit and it was found to be ~6.3 x 10^{-7} M. (Fig. S12, ESI†) Hence, the TCSPC results corroborated the DFT results and suggested that upon binding to **1**, Fe^{3+} lowers the energy of piperazine 'N' lone pair orbital and hence prohibits PET form piperazine 'N' to naphthalimide.

The absorbance and fluorescence characteristics of **1** at various concentrations of Fe^{3+} added are shown in **Fig. 3**. Upon increasing the amount of Fe^{3+}, absorption band of **1** at ~407 nm was gradually blue shifted with a slight enhancement in its molar absorption coefficient. The maximum shift was observed with the addition of 20 μM of Fe^{3+} ions (**Fig. 3a**). Under similar conditions, fluorescence intensity of **1** at ~518 nm was substantially increased with the addition of serial concentrations of Fe^{3+} ions (0-20 μM). The increment in the fluorescence intensity was linear in the range of 0.1 x 10^{-7} to 8.0 x 10^{-6} M concentration of Fe^{3+} ions (**Fig. 3b**). Binding constant of **1-Fe^{3+}** complex and Fe^{3+} ion detection limit of **1** were calculated from the fluorescence data (Fig. S13, ESI†) and are found to be 1.04 x 10^5 M^{-1} and ~3.0 x 10^{-8} M, respectively. Reversibility of **1-Fe^{3+}** complex was established using EDTA experiments (Fig. S14, ESI†). The fluorescent '**1-Fe^{3+}**' solution turned to non-fluorescent with the addition of EDTA solution and its fluorescence was regained upon addition of excess amounts of Fe^{3+}. The emission spectrum of '**1**-Fe^{3+}-EDTA' solution resembled **1** alone, indicated that the added EDTA extracted Fe^{3+} from **1-Fe^{3+}** complex and resulted in the formation of **1** and **EDTA-Fe^{3+}** complex.

Stability at physiological pH, non-toxicity and free from the interference of biologically relevant ions are the key criteria to a chemosensor for biological applications. The effect of pH on the fluorescence characteristics of **1** was estimated using acid-base titration experiments (Fig. S15, ESI†). The results revealed that emission characteristics of **1** were impassive to the variations in pH in the range of pH 4.5-10 and indicated its stability at physiological pH conditions. Moreover, the observed enhancement in the fluorescence intensity of the probe under strong acidic conditions (pH < 4) indicated that PET process is inhibited by the protonation of PET donor (piperazine 'N').[16] Further the results of the MTT assay designated that both the NIH 3T3 and W138 cells are viable (cell viability is more than 90%) even after 48h of internalization of **1** (up to 25 μM concentration) and suggested its applicability for live cell

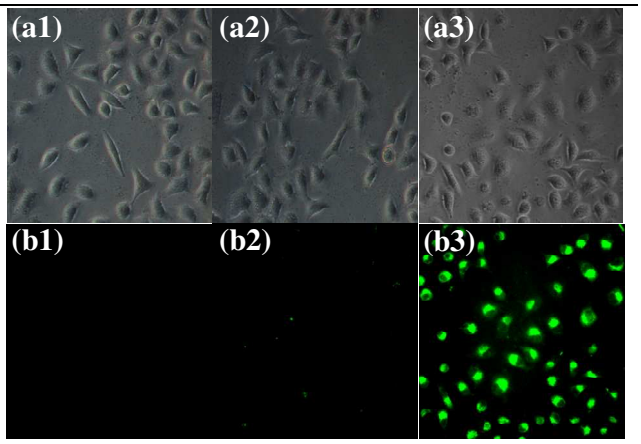

Fig. 4. Fluorescence microscopic images of W138 cells: Row 1 (**a1-a3**): bright field images, Row 2 (**b1-b3**): fluorescence images obtained using green filter. Column 1 (**a1-b1**): W138 cells alone, Column 2 (**a2-b2**): cells treated with **1** (10 μM) alone; Column 2 (**a3-b3**): cells treated with **1** (10 μM) and Fe^{3+} (10 μM).

imaging experiments (Fig. S16, ESI†). Furthermore, the cytotoxic effect of Fe^{3+} on W138 cells is also evaluated using MTT assay (Fig. S16c, ESI†). The results revealed that the W138 cells are significantly viable up to 25 μM of added Fe^{3+} ions.

Metal ion competitive experiments were performed to assess the Fe^{3+} ion detection ability of **1** in presence of other metal ions and the results suggested that probe **1** could be used to detect Fe^{3+} ions even in the presence of other competitive metal ions at excess concentrations (Fig. S17, ESI†).

After establishing high Fe^{3+} selectivity and sensitivity, non-interference from other common metal ions, broad pH stability and non-cytotoxicity of probe **1**, we have conducted live cell imaging experiments using probe **1** (**Fig. 4**). The W138 human lung fibroblast cells were used for live cell imaging experiments. Cells alone, cells incubated with only Fe^{3+} ions (10 μM) and cells incubated with only **1** (10 μM) did not show any considerable fluorescence emission when they observed under fluorescence microscope. However, upon exposing to exogenous Fe^{3+} ions (10 μM), an intense intracellular green fluorescence was observed from the probe loaded cells. Further, W138 cells loaded with **1** (10 μM) were treated with various amounts of Fe^{3+} ions (0-10 μM), corresponding fluorescence outputs were measured using a well plate reader and a calibration curve was constructed (Fig. S18a, ESI†). A clear enhancement in the fluorescence intensity of the probe loaded cells was observed even with the addition of 1 μM of Fe^{3+} ions and the fluorescence intensity was linearly increased with the amount of Fe^{3+} added (Fig. S18a, ESI†). Similarly, W138 cells loaded with **1** (10 μM) were separately incubated with Fe^{3+} ions (2.5 and 5.0 μM) and the amount of Fe^{3+} ions added was determined separately from the fluorescence outputs using the calibration curve and ICP-OES analyses (Fig. S18b and Table 2, ESI†). These results revealed the practical applicability of **1** to detect Fe^{3+} ions present in the live cells. To our knowledge, **1** is the first naphthalimide based PET fluorescent probe useful for the selective detection of Fe^{3+} ions present in the aqueous as well as biological samples in 'turn-on' fluorescence mode.

In conclusion, we have reported the first naphthalimde based Fe^{3+} selective fluorescence 'turn-on' probe that operates based on

PET mechanism for the selective detection of Fe^{3+} ions present in aqueous and biological samples. The probe is weakly fluorescent due to the photoinduced electron transfer from piperazine 'N' to naphthalimide and turned to highly fluorescent selectively with the addition of Fe^{3+} ions. The Fe^{3+}-induced reduction in the PET in probe **1** is confirmed using DFT calculations and TCSPC experiments. Probe **1** is highly selective to Fe^{3+} ions and the presence of other competitive metal ions does not affect its Fe^{3+} detection ability. The probe is stable over a wide range of pH, non-toxic under experimental conditions and could be used for the imaging of intracellular Fe^{3+} ions with its 'turn-on' fluorescence output.

Acknowledgments

One of the authors, N. R. Ch., thanks the CSIR, New Delhi, India, for CSIR-Nehru Science Postdoctoral Fellowship. P. N and V. R. K thanks CSIR, New Delhi, India, for research fellowship. Financial support from CSIR 12th plan project CSC0201 and 'INTELCOAT' is acknowledged.

Notes and references

[a]*Crop Protection Chemicals,* [c]*Inorganic and Physical Chemistry Division CSIR-Indian Institute of Chemical Technology, Tarnaka, Hyderabad-500 007, India, E-Mail: chereddynarendra@gmail.com*
[b]*Biomaterials Division, CSIR-Central Leather Research Institute, Adyar, Chennai-600 020, India*

† Electronic Supplementary Information (ESI) available: Experimental procedure for the synthesis of **1**, $^{1}H/^{13}C$ NMR, ESI-HRMS spectra of **1**, theoretical calculations, TCSPC analysis, Job plot, ESI-MS spectra of **1-Fe^{3+}** complex, binding constant and detection limit calculations, reversibility of **1-Fe^{3+}** complex, effect of pH on **1-Fe^{3+}** complex, cell viability assay and metal ion competitive experiments. See DOI: 10.1039/b000000x/

1 (a) S. J. Lippard and J. M. Berg, *Principles of Bioinorganic Chemistry*, University Science Books: Mill Valley, CA, 1994; (b) W. Kaim and B. Schwederski, *Bioinorganic Chemistry*, 2nd ed., B. G. Teubner: Stuttgart, Germany, 1995.
2 P. Aisen, M. Wessling-Resnick and E. A. Leibold, *Curr. Opin. Chem. Biol.*, 1999, **3**, 200.
3 (a) B. Halliwell and J. M. C. Gutteridge, *Methods Enzymol.,* 1990, **186**, 1; (b) B. Halliwell and J. M. C. Gutteridge *FEBS Lett.,* 1992, **307**, 108.
4 (a) A. Gaeta and R. C. Hider, *Br. J. Pharmacol.,* 2005, **146**, 1041; (b) J. P. Kehrer, *Toxicology,* 2000, **149**, 43; (c) K. V. Kowdley, *Gastroenterology,* 2004, **127**, S79; (d) M. Valko, C. J. Rhodes, J. Moncol, M. Izakovic and M. Mazur, *Chem.-Biol. Interact.,* 2006, **1**, 1; (e) M. Valko, D. Leibfritz, J. Moncol, M. T. Cronin, M. Mazur and J. Telser, *Int. J. Biochem. Cell Biol.,* 2007, **39**, 44.
5 A. Ohashi, H. Ito, C. Kanai, H. Imura and K. Ohashi, *Talanta*, 2005, **65**, 525.
6 Z.-Q. Liang, C.-X. Wang, J.-X. Yang, H.-W. Gao, Y.-P. Tiang, X.-T. Tao and M.-H. Jiang, *New J. Chem.,* 2007, **31**, 906.
7 (a) S. Lunvongsa, M. Oshima and S. Motomizu, *Talanta*, 2006, **68**, 969; (b) Z. O. Tesfaldet, J. F. van Staden and R. I. Stefan, *Talanta*, 2004, **64**, 1189; (c) D. M. C. Gomes, M. A. Segundo, J. L. F. C. Lima and A. O. S. S. Rangel, *Talanta*, 2005, **66**, 703.
8 A. Bobrowski, K. Nowak and J. Zarebski, *Anal. Bioanal. Chem.*, 2005, **382**, 1691.
9 F. Petrat, H. de Groot, R. Sustmann and U. Rauen, *Biol. Chem*., 2002, **383**, 489.
10 (a) S. Fakih, M. Podinovskaia, X. Kong, H. L. Collins, U. E. Schaible and R. C. Hider, *J. Med. Chem*., 2008, **51**, 4539; (b) C. Qin, Y. Cheng, L.Wang, X. Jing and F.Wang, *Macromolecules*, 2008, **41**, 7798; (c) J. Yao, W. Dou, W. Qin and W. Liu, *Inorg. Chem. Commun*., 2009, **12**, 116; (d) C. R. Lohani and K.-H. Lee, *Sens. Actuators, B*, 2010, **143**, 649; (e) X. Wu, B. Xu, H. Tong and L. Wang, *Macromolecules*, 2010, **43**, 8917; (f) Y. Qi, N. Li, X. Xia, J. Ge, J. Lu and Q. Xu, *Mater. Chem. Phys*., 2010, **124**, 726; (g) M. Kumar, R. Kumar and V. Bhalla, *Tetrahedron Lett*., 2010, **51**, 5559; (h) S. Smanmoo, W. Nasomphan and P. Tangboriboonrat, *Inorg. Chem. Commun*., 2011, **14**, 351; (i) Z.-X. Li, L.-F. Zhang, W.-Y. Zhao, X.-Y. Li, Y.-K. Guo, M.-M. Yu and J.-X. Liu, *Inorg. Chem. Commun*., 2011, **14**, 1656; (j).C. Queiros, A. M. G. Silva, S. C. Lopes, G. Ivanova, P. Gameiro and M. Rangel, *Dyes Pigm*., 2012, **93**, 1447.
11 (a) Y. Xiang and A. Tong, *Org. Lett*., 2006, **8**, 1549; (b) J. Mao, Q. He and W. Liu, *Talanta*, 2010, **80**, 2093; (b) B. Wang, J. Hai, Z. Liu, Q. Wang, Z. Yang and S. Sun, *Angew. Chem. Int. Ed.*, 2010, **49**, 4576; (c) A. J. Weerasinghe, C. Schmiesing, S. Varaganti, G. Ramakrishna and E. Sinn, *J. Phys. Chem. B*, 2010, **114**, 9413; (d) L.-F. Zhang, J.-L. Zhao, X. Zeng, L. Mu, X.-K. Jiang, M. Deng, J.-X. Zhang and G. Wei, *Sens. Actuators, B*, 2011, **160**, 662; (e) Jy D. Chartres, M. Busby, M. J. Riley, J. J. Davis and P. V. Bernhardt, *Inorg. Chem*., 2011, **50**, 9178; (f) M. She, Z. Yang, B. Yin, J. Zhang, J. Gu, W. Yin, J. Li, G. Zhao and Z. Shi, *Dyes Pigm*., 2012, **92**, 1337; (g) A. Sikdar, S. S. Panja, P. Biswas and S. Roy, *J. Fluoresc*., 2012, **22**, 443; (h) Z. Aydin, Y. Wei and M. Guo, *Inorg. Chem. Commun*., 2012, **20**, 93; (i) N. R. Chereddy, S. Thennarasu and A. B. Mandal, *Dalton. Trans.,* 2012, **41**, 11753; (j) J. Mao, L. Wang, W. Dou, X. Tang, Y. Yan and W. Liu, *Org. Lett*., 2007, **9**, 4567; (k) N. R. Chereddy, K. Suman, P. S. Korrapati, S. Thennarasu and A. B. Mandal, *Dyes Pigm.*, 2012, **95**, 606; (l) N. R. Chereddy, S. Thennarasu and A. B. Mandal, *Analyst,* 2013, **138**, 1334; (m) N. R. Chereddy, K. Saranraj, A. K. Barui, C. R. Patra, V. J. Rao and S. Thennarasu, *RSC Adv.,* 2014, **4**, 24324.
12 (a) H. Zheng, X.-Q. Zhan, Q.-N. Bian and X.-J. Zhang, *Chem. Commun.,* 2013, **49**, 429; (b) X. Chen, T. Pradhan, F. Wang, J. S. Kim and J. Yoon, *Chem. Rev*., 2012, **112**, 1910.
13 (a) R. M. Duke, E. B. Veale, F. M. Pfeffer, P. E. Kruger and T. Gunnlaugsson, *Chem. Soc. Rev*., 2010, **39**, 3936; (b) P. A. Panchenko, O. A. Fedorova and Y. V Fedorov, *Russ. Chem. Rev*., 2014, **83,** 155.
14 (a) C.-H. Li, F. Xu, Y.-F. Li, K. Zhou and Y. Zhou, *Anal. Chim. Acta*, 2012, **717**, 122; (b) R. Yang, X. F. Guo, W. Wang, Y. Zhang and L. Jia, *J. Fluoresc*., 2012, **22**, 1065; (c) W. Wang, Q. Wen, Y. Zhang, X. Fei, Y. Li, Q. Yang and X. Xu, *Dalton Trans*., 2013, **42**, 1827.
15 H. Lu, S. Zhang, H. Liu, Y. Wang, Z. Shen, C. Liu and X. You, *J. Phys. Chem. A,* 2009, **113**, 14081.
16 S. Iyoshi, M. Taki, and Y. Yamamoto, *Inorg. Chem*., 2008, **47**, 3946.